Computational analysis of the effect of [Tea][Ms] and [Tea][H_2PO_4] ionic liquids on the structure and stability of A$\beta(17-42)$ amyloid protofibrils

D. Gobbo,[(1)] A. Cavalli,[(1,2)], P. Ballone,[(3,4)] A. Benedetto[(3,4,5,6)]

(1) Computational and Chemical Biology, Fondazione Istituto Italiano di Tecnologia, Genova, Italy

(2) Department of Pharmacy and Biotechnology (FaBiT), University of Bologna, Bologna, Italy

(3) School of Physics, University College, Dublin, Ireland

(4) Conway Institute for Biomolecular and Biomedical Research, University College, Dublin, Ireland

(5) Department of Sciences, University of Roma Tre, Rome, Italy and

(6) Laboratory for Neutron Scattering, Paul Scherrer Institute, Villigen, Switzerland

Abstract

Experimental studies have reported the possibility of affecting the growth/dissolution of amyloid fibres by the addition of organic salts of the room-temperature ionic-liquids family, raising the tantalizing prospect of controlling these processes at physiological conditions. The effect of [Tea][Ms] and [Tea][H_2PO_4] at various concentrations on the structure and stability of a simple model of Aβ42 fibrils has been investigated by computational means. Free energy computations show that both [Tea][Ms] and [Tea][H_2PO_4] decrease the stability of fibrils with respect to isolated peptides in solution, and the effect is significantly stronger for [Tea][Ms]. The secondary structure of fibrils is not much affected, but single peptides in solution show a marked decrease in their β-strand character, and an increase in α-propensity, again especially for [Tea][Ms]. These observations, consistent with the experimental picture, can be traced to two primary effects, i.e., the different ionicity of the [Tea][Ms] and [Tea][H_2PO_4] water solutions, and the remarkable affinity of peptides for $[Ms]^-$ anions, due to a multiplicity of H-bonds.

† Corresponding author: dorothea.gobbo@iit.it

I. INTRODUCTION

The current broad research activity on organic ionic compounds of the room-temperature ionic liquids family[1] (RTIL) has sparked interest in their potential applications in biotechnology,[2] pharmacology[3,4] and biomedicine.[5,6] In this context, the first experimental observation[7] of RTILs affecting the structure, stability and fibrillation kinetics of amyloid fibres has raised the tantalising prospect of controlling and perhaps reversing the self-assembly of peptides and proteins into amyloids.

Over the years, many studies have reported similar results concerning several types of amyloids and RTILs.[8,9] In the broad health sciences context, the results of two experimental papers have attracted considerable interest, since they report the effect of RTILs on the fibrillation kinetics of the Aβ peptides,[10,11] which form amyloid plaques found in the brain of people affected by Alzheimer's disease[12] (See also Ref. 13), and are implicated in other degenerative conditions such as inclusion body myositis and cerebral amyloid angiopathy.[14] The focus of Ref. 10, in particular, was on Aβ40 and triethylammonium methanesulfonate [Tea][Ms], a protic ionic liquid[15,16] which was already known to stabilise the folded state of hen egg white lysozyme,[17] preventing its fibrillation. In Ref. 10, the secondary structure of Aβ40 and of its aggregates was probed by circular dichroism (CD),[18] the formation of fibrils detected by fluorescence of the thioflavin T (ThT) dye,[19–21] and the morphology of mature fibres was investigated by transmission electron microscopy. Up to 50 wt% [Tea][Ms] concentration, the formation of β sheets was apparent. At higher concentration, i.e., between 70 and 80 wt% of RTIL, the structure of Aβ peptides turned to α-helix, preventing fibrillation, while at 90 wt% [Tea][Ms] concentration, the Aβ40 peptide lacked any structure, and, again, fibrillation did not take place. Further measurements on Aβ16-22 gave similar results, confirming that this core segment of Aβ40 and Aβ42 provides a convenient model for the aggregation of Aβ peptides. Then, Aβ16-22 became the main subject of Ref. 11, investigating the effect on fibrillation of six protic ionic liquids (pILs), having $[Tea]^+$ as their common cation. It was found that the fibrillation kinetics follows an inverse Hofmeister series,[22] being faster for stronger kosmotropic compounds such as [Tea][HSO_4] and [Tea][H_2PO_4] than for more chaotropic compounds such as [Tea][Ms]. This observation contrasts with the original Hofmeister ordering in which stronger kosmotropic compounds display an enhanced ability to salt-out peptides and proteins, stabilising their native folding and preventing fibrillation.

To provide microscopic insight into these macroscopic observations, atomistic simulations have been carried out. Because of the complexity and time scale of fibrillation, whose lag time can extend up to several days, simulations cannot aim at reproducing directly the experimental phenomena. Instead, we aim at analysing features and properties that affect the outcome of experimental results.

The planning of our work has been eased by a vast literature on modeling and simulation of amyloid fibres (See Ref. 23 for a review, and Ref. 24 for a very recent study). The present simulations, in particular, have been inspired by a recent study of the stability of Aβ protofibrils[25] computing the free energy cost of separating one peptide from a protofibril. Assuming equilibrium and reversibility, the same information can be used to characterise the reverse process of fibril growth. While Ref. 25 aimed at estimating the effect of mutations on the stability and fibrillation kinetics, we set out to investigate by the same approach the effect of different water/organic electrolyte solutions on the same properties.

The main RTIL target of the present study has been [Tea][Ms] because of its ability to prevent fibrillation.[10] A single sample containing [Tea][H_2PO_4] at $\sim$ 25 wt% concentration has also been simulated to contrast the [Tea][Ms] results with those of a system expected to enhance the fibrillation kinetics.[11] A further comparison is provided by a sample whose watery environment consists of a dilute NaCl water solution. A few complementary aspects have been analysed in our study. Since dissolving amyloid Aβ fibrils is of such practical relevance, we investigated whether [Tea][Ms] at low/medium concentration could degrade protofibrils. To make closer contact with the experimental results, we also investigated the effect of [Tea][Ms] and [Tea][H_2PO_4] on the secondary structure of a protofibril, and we computed the free energy profile connecting a single Aβ peptide in solution to the same peptide bound to the extremity of a formed protofibril. Moreover, to probe the very early stages of protofibril formation, single peptides and peptide dimers in solution have been simulated. Last but not least, to extend our analysis of the experimental results, we also investigated the binding of the ThT dye to the protofibril in [Tea][Ms] / water solution. To clarify the relation between the experimental observations and the results of the simulations presented in this work, it might be worth emphasizing that the measurements of Ref. 10,11 start with a population of peptides in solution, and focus on the fibrils' aggregation stage, but, at variance from other studies on different amyloids, do not test the ability of RTILs to dissolve pre-formed fibrils. Limited information on the ability of neat [Tea][Ms] to slowly dissolve Aβ40 fibrils, however, is reported in Ref. 13, stating that up to late

stages of dissolution the morphology of the residual fibrils is relatively unchanged.

The computational results show several points of contact with the experimental picture. The effect of [Tea][Ms] and [Tea][H_2PO_4] on the protofibril secondary structure, for instance, parallels the trends observed in experiments. Moreover, addition of both salts decreases the stability of the protofibril, and the effect is larger for [Tea][Ms]. Many aspects, however, still escape a direct microscopic understanding by atomistic simulation, and require further elaboration and inference to gain insight into the experimental picture. First of all, the range of RTIL concentrations considered in our simulations, although broad, has been limited by the marked nanostructuring of the RTIL / water solutions, affecting the reproducibility of the results, and by exceedingly slow kinetics at the highest salt concentrations. This problem, in particular prevented us from investigating salt concentrations above 80 wt%, at which the different effect of [Tea][Ms] and [Tea][H_2PO_4] become most apparent. Therefore, a required assumption of our study is that the salt-water-peptide interactions responsible for the effects seen at very high concentration are already at play and can be identified in the range of concentrations we considered.

II. METHOD

The starting point for our study is provided by the work of Lemkul and Bevan[25] on the structure and stability of Aβ nanofibrils. In our simulations we adopt the same model consisting of 5 peptides (A to E) characterized by the presence of intact salt bridges (see Fig. 1 (a)). Following again Ref. 25 we refer to this minimal model as a protofibril, while using fibril to denote more general and especially experimental systems. It might be worth pointing out that in this model, based on the experimental NMR structure of Ref. 26, the β-strands run parallel to each other, while they are identified as anti-parallel in the experimental papers of Ref. 10,11,13.

Following the reference set-up, the parameters from the GROMOS96 53A6 has been chosen to describe the protofibril. The N-terminus of each peptide has been capped with a neutral acetyl group thus approximating the full-length Aβ42 peptide. The C-terminus of each peptide was deprotonated, and left negatively charged. All other titratable groups have been prepared in their standard protonation state at physiological pH. The protofibril was placed in an orthorhombic box of flexible simple point charge (SPC) water. In the computation of Ref. 25 on top of neutralizing counter-ions, a concentration of 100 mM NaCl was added to the system,

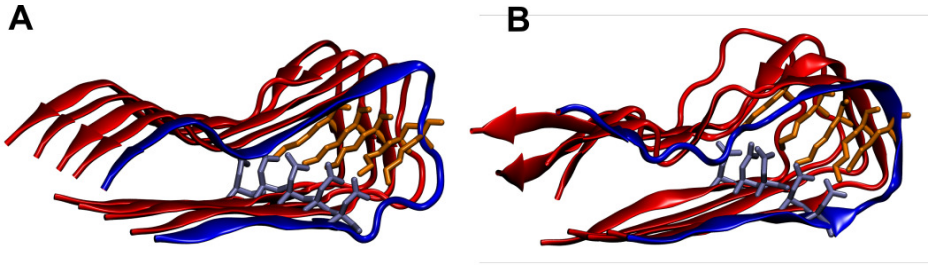

FIG. 1: Simulation snapshots of the Aβ17-42 protofibril: (a) in the control dilute [Na][Cl] solution; (b) in the [Tea][Ms] water solution at 25 wt% RTIL concentration. The β_1 and β_2 strands are at the bottom and at the top of each protofibril, respectively.

using the ion force field which is part of GROMOS96 53A6. In our study, the $[Tea]^+$, $[Ms]^-$ and $[H_2PO_4]^-$ ions, whose structure is outlined in Fig. 2 have been considered as well. For these species, we relied on the Gromos parametrisation provided by the on-line Automated Topology Builder (ATB) tool.[27] We adopted a generic force field such as Gromos for the ions instead of an RTIL-specific one to achieve an unbiased description of the salt, water and peptide components of the simulated system. A preliminary validation of the force field has been obtained by performing density functional computations for the single ions and neutral ion pairs (see Sect. I of the Supporting Information (SI) document), comparing geometries, RESPA atomic charges and vibrational modes with the results provided by the empirical force field. The topology files for the ions are given as SI. In the last part of the present study, the binding of the thioflavin-T dye to the protofibril in a [Tea][Ms] / water solution has been investigated. Thioflavin-T, which is a cation (and in what follows it will be indicated as ThT^+) at the conditions of experiments and of our simulations, has been modeled with a Gromos parametrisation provided again by ATB. In the simulated samples, ThT^+ replaced one of the original RTIL cations.

A. Molecular dynamics simulation

The core of the computational plan has been represented by molecular dynamics simulations in the NVT and NPT ensembles for systems consisting of up to 35000 atoms, simulated for hundreds of ns at $T = 300$ K.

All MD simulations were performed using GROMACS version 2016.5. Short-range electrostatic interactions were treated with the Verlet cut-off scheme and long-range ones with the

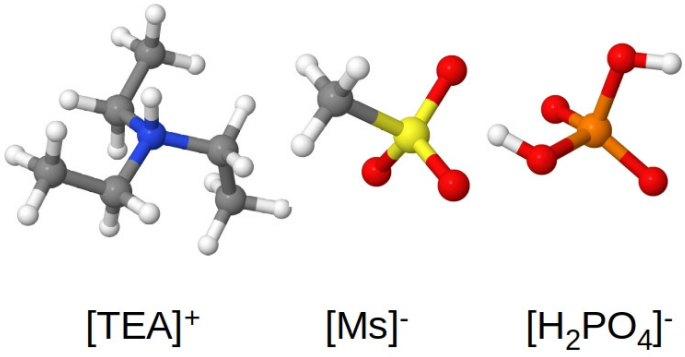

FIG. 2: Structure of the $[Tea]^+$, $[Ms]^-$ and $[H_2PO_4]^-$ ions.

Particle Mesh Ewald (PME)[28] method. In both cases, the cut-off was fixed at 1 nm. Periodic boundary conditions (pbc) were applied. The steepest descent algorithm was applied to energy minimize the system. For all MD simulations, Langevin dynamics with a time constant for coupling equal to 2.0 ps was used. For simulations performed in the NPT ensemble, the average pressure of the system was equilibrated to 1 atm using the Parrinello-Rahman barostat. The integration time step was limited to 1 fs mainly because of the fast vibrational dynamics of the flexible 3-points water model.

Trajectories have been analysed using homemade computer programs, together with popular visualisation tools such as Jmol[29] and VMD.[30]

B. Steered MD (sMD) and umbrella sampling (US)

The last configurations of the NPT MD simulations of the previous subsection provided the well equilibrated input for the subsequent analysis focusing on the stability of the protofibril in different solutions, carried out by steered molecular dynamics (sMD) and by umbrella sampling (US) computations.

All the putative solvation paths of the two peptides at the edge of the protein system, i.e. peptide A and E, were generated by sMD, fixing the positions of peptides B and D, respectively. As reaction coordinate, we used the projection along the longest side of the orthorhombic simulation cell of the distance between the two centres of mass of the pulled peptide and the adjacent peptide. The peptide separation was driven by a pulling force with a force constant of

1,000 kJ mol^{-1} nm^{-2} applied to the centre of mass of the pulled peptides and directed towards the solvent. The rate of change of the reference position was fixed at 0.005 nm ps^{-1}. The value of the reaction coordinate was used to identify a sizeable number (> 30) of windows spaced by ~ 0.1 nm when the residual protofibril and the pulled peptide are close to each other. A spacing of 0.2 nm was considered when the pulled peptide reached a complete solvated state.

For each umbrella window, equilibration lasted 10 ns whereas statistics was accumulated for 36 ns. The harmonic force constant used in the umbrella sampling simulations was varied from 1000 up to 5000 kJ mol^{-1} nm^{-2} depending on the relative position of the two peptides to improve the sampling of the transition state region. The potential of mean force (PMF) was reconstructed using the weighted histogram analysis method (WHAM[31]) as implemented in Gromacs version 2017.5. Error bars have been estimated by a bootstrap analysis.[32]

III. RESULTS

A first stage of plain MD computations have been carried out for the series of samples listed in Tab. I, consisting of the protofibril briefly introduced in the previous section and of a water/electrolyte solution spanning a wide range of salt concentrations. The total simulation times reported in the same table have been divided a posteriori into an equilibration and a production stage upon verifying the stabilisation of estimators for the energy, volume and structure. The focus of the present study is on [Tea][Ms] which, according to Ref. 10,11, at high concentration prevents the fibrillation of Aβ peptides, while a single [Tea][H_2PO_4] sample at medium salt concentration (SAMP5) has been simulated to provide a comparison with a compound that, again according to Ref. 11, favours fibrillation. The two RTILs share the same $[Tea]^+$ cations, and the two anions are known for their ability to form multiple H-bonds. In particular, $[Ms]^-$ can only accept H-bonds, while $[H_2PO_4]^-$ can act simultaneously as a proton acceptor and donor.[33] A further comparison is provided by SAMP0, which, at low [Na][Cl] concentration, represents the control state of the protofibril, unperturbed by the addition of the organic ionic compounds.

As already stated, the protofibril is the same considered in Ref. 25, made of 5 peptides connected primarily by H-bonds. Each peptide consists of residues 17-42 in the Aβ42 sequence. Considering also the ACE group that saturates the N terminus, each peptide contains 27 residues, whose identity and numbering is listed in Fig. 3. In what follows, the numbering

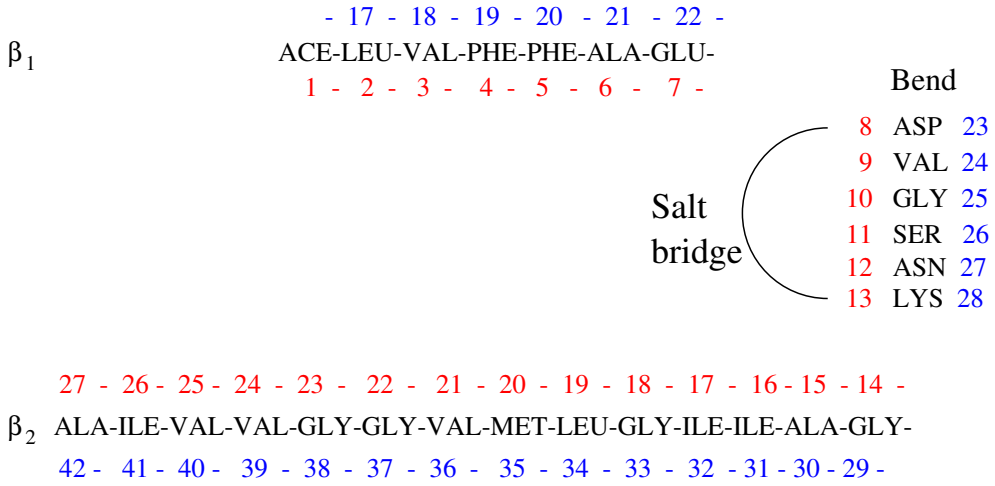

FIG. 3: Numbering of residues in the fibril according to: (blue) the Aβ42 sequence, and (red) the reduced Aβ17-42 sequence.

TABLE I: Composition of the water/electrolyte environment surrounding the protofibril given by the number (#) of water molecules, of cations and anions. The composition in wt% refers to the proportion of IL in the solution, excluding the protofibril. The total simulation time τ (ns) for each sample is given in the last column. It does not include the steered MD and US stages.

Sample	# H_2O	# $[Tea]^+$	# $[Ms]^-$	# $[H_2PO_4]^-$	# $[Na]^+$	# $[Cl]^-$	wt%	τ (ns)
SAMP0	10675	0	0	0	31	21	0.6	333
SAMP1	10621	31	21	0	0	0	3	153
SAMP2	10420	127	117	0	0	0	11	155
SAMP3	8075	255	245	0	0	0	25	368
SAMP4	1584	1022	1012	0	0	0	88	862
SAMP5	8075	255	0	245	0	0	26	180

corresponds to the sequence of amino acids in Aβ42.

Each peptide can be divided into the β_1 (LEU17 to GLU22) and β_2 (GLY29 to ILE41) strands, and a bend (ASP23 to LYS28) connecting them. In the fibril, the first two strands arrange themselves into short parallel β-sheets, and the bend, starting at residue ASP23, gives the fibril the shape of an elongated *c*.

The structure of the fibril and its interaction with its environment are determined by several

features. First, each of the five peptides carries three anionic (GLU22, ASP23, ALA42) and one cationic (LYS28) residues, resulting in a total net charge of $-2e$ per peptide, or $-10e$ for the simulated protofibril. Two of the charged residues, i.e., ASP23 and LYS28 form a salt bridge, bound by Coulomb forces and a hydrogen bond. The role of this salt bridge in stabilising the shape of the protofibril is apparent from its persistence in the trajectories of all simulated systems. The net charge of the protofibril is neutralised by a corresponding imbalance in the number n_+ of cations and n_- of anions from the salt dissolved in solution, with $n_+ = n_- + 10$. Moreover, the structure of the β_1 and β_2 sheets is primarily determined by the number and distribution of intra- and inter-peptide H-bonds, whose properties are discussed below. Close contact of aromatic rings in PHE19 and PHE20 are also important, but more difficult to quantify. Last but not least, Coulomb interactions of the peptides with the salt ions and H-bonding with both ions and water also play crucial roles.

As it is generally the case for amyloid aggregates, the protofibril has a predominantly hydrophobic signature, and this character is particularly apparent for the inside of the protofibril, contributing to enhance the stability of its c shape.

A. Preliminary analysis of the electrolyte / water solutions

The different effect of [Tea][Ms] and [Tea][H_2PO_4] on the fibrillation kinetics of Aβ peptides has been interpreted in Ref. 11 as reflecting their different position along the Hofmeister series.[34] More precisely, as stated in the Introduction, according to Ref. 11 the fibrillation of Aβ peptides follows an inverse Hofmeister series, with [Tea][Ms] (more chaotropic) preserving the folded form, and [Tea][H_2PO_4] (more kosmotropic) favouring denaturation and fibrillation.

Since the Hofmeister series is extensively referred to in experimental papers, we discuss in Sec. II of SI how far it is reflected in the results of atomistic simulations. The results show that, at this microscopic level, the Hofmeister series concept is elusive, especially in comparing organic salts[35,36] whose size and charge are rather similar.

A simpler account (See Tab. S2 in SI for the complete picture) of the effect of adding salts to water is that up to the [Tea][Ms] concentration of SAMP3, 75% of the $[Tea]^+$ ions donate one H-bond to water, and each $[Ms]^-$ ion accepts nearly 4 H-bonds from water. In SAMP5 with 25 wt% [Tea][H_2PO_4], only 15% of the $[Tea]^+$ ions donate one H-bond to water, but 70% of $[Tea]^+$ ions donate a H-bond to $[H_2PO_4]^-$, pointing to weaker dissociation of [Tea][H_2PO_4] in

water. Moreover, each $[H_2PO_4]^-$ ions accepts ~ 3 H-bonds from water. As a result, the H-bond capability of water and ions is nearly equally saturated in all samples (with larger deviations in SAMP4), but the distribution of acceptance and donation among species changes in the different samples, possibly underlying the different fibrillation behaviour of Aβ's in the corresponding solutions. In particular, the observed weaker dissociation in water of [Tea][H_2PO_4] with respect to [Tea][Ms], corresponding to a lesser ionic character, is a first major difference between the two compounds.

Animations of simulation trajectories show that in all samples, the solution on average appears homogeneous. However, large amplitude dynamic fluctuations in the distribution of ions are observed in SAMP3 (see Fig. S2 in SI) and even more in SAMP5, that could suggest either the proximity of a solubility gap for the salt / water system at salt concentrations > 30 wt%, or a marked nanostructuring,[37,38] due to the different solubility of the $[Ms]^-$ and $[H_2PO_4]^-$ anions (both rather hydrophilic) and of the $[Tea]^+$ cation (much less hydrophilic).[39] It is worth emphasizing, however, that fluctuations are not static, as it would be the case for a genuine phase separation. Detailed and extensive simulations,[40] in fact, confirm the apparent nanostructuring of the [Tea][Ms] and [Tea][H_2PO_4] / water solutions and disprove the phase separation of salt ad water in these systems. In any case, the large composition fluctuations on length scales comparable to the protofibril size, and their long relaxation times due to nanostructuring are the reasons why our investigations did not cover a wider range of concentrations. In real systems, nanostructuring could be an additional factor influencing the effect of organic salts on the amyloid fibrils.[41,42] Because of the inhomogeneous perturbation represented by the protofibril, however, these aspects are difficult to unambiguously characterise in our relatively small samples and short simulation times.

An additional aspect of the solvent environment that is relevant for the kinetics of fibrillation and dissolution is the diffusion of water and ions in the various samples. The results are summarised in Tab. II. As expected, the fluidity of the samples decreases with increasing RTIL concentration. However, up to the high [Tea][Ms] concentration of SAMP4, water and ions display flow-like (i.e., not jump-like) diffusion, as shown by the plot of their mean square displacement as a function of time reported in Fig. S3 of SI. More in detail, the diffusion constant of all species is moderately affected by salt up to the 25 wt% concentration of SAMP3 and SAMP5. Remarkably, however, water has the same diffusion constant in SAMP3 and SAMP5, but both $[Tea]^+$ and $[H_2PO_4]^-$ diffuse less than the ions in SAMP3, reflecting the

higher association in water of [Tea][H_2PO_4]. At the 88 wt% concentration in [Tea][Ms] of SAMP4, diffusion is reduced by three orders of magnitude. If one interprets this ratio in terms of the approximate Stokes-Einstein relation, this result implies that viscosity increases by three orders of magnitude from SAMP0 or SAMP1 to SAMP4, greatly limiting the rate of processes such as the addition of peptides to a growing fibril. In all samples, the decrease of diffusion with increasing salt concentration arises from several effects, including the high mass of the RTIL ions, the cage effect created by these bulky ions, and the number of H-bonds shared by water and ions, that further decrease diffusion.

B. Free energy computations

A quantitative assessment of thermodynamic stability and formation/dissolution kinetics of fibrils has been sought by applying the combined steered-MD and umbrella sampling approach described in Sec. II B. Using these methods, the free energy profile along a reaction coordinate connecting the 5-peptide protofibril to the 4-peptide plus one isolated peptide in solution has been computed for the control sample SAMP0 as well as for SAMP3 and SAMP5. In all cases the computation has been repeated twice, separating in turn peptide A and peptide E from the centre of mass of the closest peptide in the original protofibril, i. e., B for peptide A, and D for peptide E. The same computation has been attempted for SAMP4, but the US stage did not converge to a reliable free energy profile, apparently because of the high viscosity of the solution.

At the steered MD stage, the force required to separate peptide A or peptide E from the protofibril has been determined as a function of the reaction coordinate (See Fig. S8 in SI). The integral of the force over the distance, however, is not a reliable estimator of the change in free energy of the protofibril, since it depends on the non-vanishing pulling velocity. To obtain a quantitative estimate of free energy differences and of the potential of mean force, the umbrella sampling step has been carried out, using intermediate configurations obtained by the steered MD to initialize the umbrella sampling windows. Each free energy profile has been computed using more than 30 US windows. Since each window has been equilibrated for 10 ns and production runs lasted 36 ns, each profile required ~ 1.5 μs to be determined, and the full set of six profiles required 9 μs. Despite this large effort, a few details have not been fully resolved by the computation. Because of the long unconstrained MD simulations (see Tab. I)

TABLE II: Diffusion constant of water and ions in the simulated samples. Data in $cm^2\ s^{-1}$. Error bars implicitly given by the number of digits.

	SAMP0	SAMP1	SAMP2	SAMP3	SAMP4	SAMP5
Water	$2.45\ 10^{-5}$	$2.25\ 10^{-5}$	$1.88\ 10^{-5}$	$1.26\ 10^{-5}$	$4.5\ 10^{-8}$	$1.26\ 10^{-5}$
Cation	$2.50\ 10^{-6}$	$4.90\ 10^{-6}$	$4.31\ 10^{-6}$	$2.96\ 10^{-6}$	$4.25\ 10^{-9}$	$6.19\ 10^{-7}$
Anion	$2.40\ 10^{-6}$	$5.33\ 10^{-6}$	$4.92\ 10^{-6}$	$3.03\ 10^{-6}$	$4.77\ 10^{-9}$	$1.89\ 10^{-7}$

TABLE III: Free energy barrier ΔF (kcal/mol) to detach peptide A or peptide E from the protofibril in the control samples and in two samples with [Tea][Ms] or [Tea][H_2PO_4]. The error bar is of the order of 1 kcal/mol in all cases.

Sample	$\Delta F(A)$	$\Delta F(E)$	$\Delta F = \frac{1}{2}[\Delta F(A) + \Delta F(E)]$
SAMP0	37.4	-	37.4
SAMP3	16.6	16.1	16.3
SAMP5	25.2	21.8	23.5

preceding the SMD stage, the protofibril orientation at the beginning of SMD is not necessarily aligned with the long side of the orthorhombic simulation cell. As a consequence, pbc may interfere with the full determination of the free energy profile. In the case of pulling peptide E from the the benchmark case SAMP0, this problem prevented us from obtaining a profile comparable to those of the other cases, leaving us with the profile for peptide A in SAMP0 as the only benchmark. Fortunately, in all the other cases the limitation due to pbc has been a minor one, and this stage of the computation provided a largely complete picture of the RTIL effect on the free energy profiles.

The computation for SAMP0, whose results are reported in Fig. 4 and in Tab. III, has been carried out primarily to validate the computational set-up by comparison with the data of Ref. 25. Fair agreement is found for peptide A, which has been considered both in Ref. 25 and in the present computation. In particular, ΔF turns out to be 37.4 kcal/mol in our computations, while it is reported as 50.5 kcal/mol in Ref. 25. Part of the discrepancy might be due to the different mesh along the reaction coordinate used to determine ΔF. Most of the difference, however, is likely to be due to the different sampling time (10 ns per window in Ref. 25, $10 + 36$ ns per window in our computation), since the equilibration of the peptide in solution at the longest separations from the protofibril is certainly a demanding task (see also Sec. III E below).

This interpretation is supported by the fact that the estimate of ΔF decreased from the early to the late stages of sampling. Nevertheless, the results of our computations agree with those of the previous study in finding that a large free energy change $\Delta F \sim 40$ kcal/mol prevents the separation of peptide A in SAMP0, showing that, in very dilute solutions, even the small protofibril is beyond the critical nucleation size. Moreover, the profile is monotonic, showing that addition of peptides takes place without lag time, at least at the (very high, compared to experiments) peptide concentration of the simulated samples.

The results for SAMP3 and SAMP5 are illustrated in Fig. 4, and Tab. III summarises the free energy barrier ΔF preventing the separation of either peptide A or peptide E in SAMP3 or SAMP5. Since, as we discuss below, most of the changes in ΔF are due (see below) to differences in the solvation of the detached peptide, the free energy profiles in Fig. 4 have been aligned setting to a common zero the free energy of peptides in their aggregated state, irrespective of the solution. Needless to say, this assumption is only approximatively justified, since the different salt / water solutions will affect in a slightly different way also the free energy of peptides bound to the protofibril.

Pulling peptide A or peptide E from the protofibril, bringing them to a fully solvated state, requires the same free energy $\Delta F(A) = \Delta F(E)$, since the solvated state of the peptide is the same, and the remaining 4-peptide protofibril is fully equivalent in the two cases. This symmetry requirement is satisfied to good accuracy in SAMP3, but somewhat violated (by 3.4 kcal/mol, or 15%) in SAMP5. Part of the difference might be due to some unidentified systematic error. However, we think that most of the difference might reflect the nanostructuring of the [Tea][H_2PO_4] / water solution (See Ref. 40), possibly making the two protofibril terminations inequivalent on the simulation time scale. Nanostructuring in SAMP5, in particular, is stronger than in SAMP3, and the (slowly fluctuating) inhomogeneous distribution of salt around the protofibril is apparent already from snapshots of SAMP5. Then, the long relaxation times of composition fluctuations on multi-ns scales might exceed the simulation times. However, the $\sim$ 15 % discrepancy between $\Delta F(A)$ and $\Delta F(E)$, although significant, does not change the qualitative picture provided by our free energy computations. In practice, to resolve the uncertainty, we average the free energy barrier to detachment of peptide A and peptide E setting $\Delta F = [\Delta F(A) + \Delta F(E)]/2$, accounting in this way for long-time-scale cancellation of every difference between the two protofibril terminations.

The most important quantitative result reported in the figure and in the table is that both

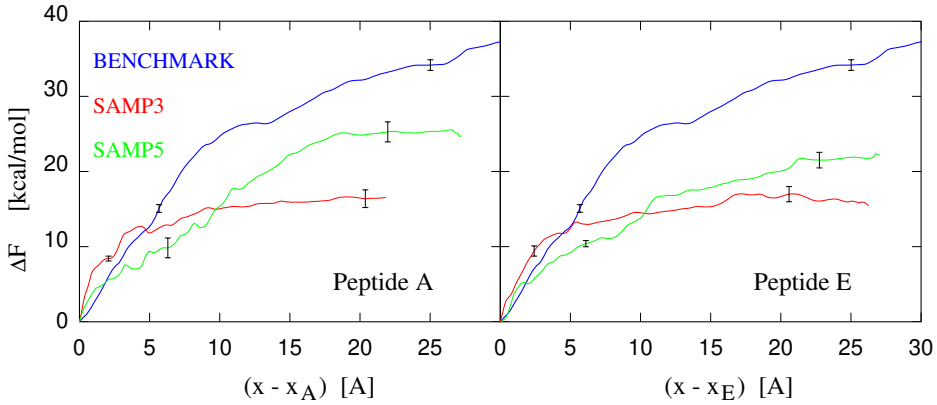

FIG. 4: Free energy profile along a reaction coordinate corresponding to the separation of peptide A or peptide E from the remaining four peptides in the protofibril (see text). Representative error bars are reported.

salts decrease substantially the stability of the protofibril, as measured by the free energy cost of detaching one peptide from either terminations. Moreover, the decrease of ΔF is more significant for [Tea][Ms] at the SAMP3 concentration than for [Tea][H_2PO_4] at the nearly equivalent concentration of SAMP5. The free energy change for dissolution, in particular, is decreased by 21.1 kcal/mol or $\sim 35\ k_BT$ by the addition of [Tea][Ms] in SAMP3, and by 13.9 kcal/mol or $\sim 23\ k_BT$ by the addition of [Tea][H_2PO_4] in SAMP5. Both at the conditions of SAMP3 ([Tea][Ms]) and SAMP5 ([Tea][H_2PO_4]), therefore, the density of solvated peptides in equilibrium with the protofibril will increase by many orders of magnitude with respect to the control solution, but the concentration of single peptides dissolved in [Tea][H_2PO_4] / water at 25 wt% salt concentration remains ~ 5 orders of magnitude lower than in [Tea][Ms] / water at the same concentration.

The slow solubilisation of peptides from the protofibril terminations suggested by the simulations, without apparent change of morphology for the residual protofibrils, is consistent with the results of Ref. 13 for Aβ40 in pure [Tea][Ms]. Even in our [Tea][Ms] / water SAMP3, $\Delta F >> 0$, and destabilisation of protofibrils is apparently far from complete, possibly because of the moderate salt concentration. Simple extrapolation to salt concentrations > 80 wt% could easily account for the complete dissolution of fibrils in [Tea][Ms] / water solutions, and for the

persistence of (partially destabilised) fibrils in [Tea][H_2PO_4] / water solutions, as seen in the experiments.

Needless to say, the thermodynamic picture has to be complemented with the kinetic aspects, especially since the system viscosity increases significantly at high [Tea][Ms] and [Tea][H_2PO_4] concentrations, greatly decreasing the fibrillation rate.[43] The role of viscosity is easy to rationalise, taking into account that at the peptide concentrations of the experiment[10,11,13], the addition of peptides to the fibril is likely to be a diffusion-limited reaction.

C. The overall protofibril geometry

The results on the thermodynamic stability of the protofibril presented in the previous section have been complemented by a detailed analysis of structural and bonding properties of the protofibril in all the simulated samples.

The first qualitative assessment of the effect of the [Tea][Ms] and [Tea][H_2PO_4] on the structure and stability of Aβ nanofibrils has been carried out by analysing the results of the equilibrium NPT simulations of samples consisting of one nanofibril, water and ions at $T = 300$ K, that, in the development of our study, preceded the sMD and US analyses already discussed. Animations of the simulation trajectories at the atomistic level do not show any major effect of the RTIL ions on the protofibril shape and dynamics. In particular, no change of shape can be perceived by visual inspection, and no peptides ever separate from each other in all samples. Wide-elongation fluctuations of the peripheral A and E peptides are visible in SAMP3 and SAMP5 at $\sim$ 25 wt% concentration of RTIL, but they concern mainly their β_2 strand. As expected, in all samples the bend segment of each peptide is more flexible than β_1 and β_2. In SAMP4, whose [Tea][Ms] concentration is 88 wt%, the motion of the protofibril is limited by the high viscosity of its electrolyte / water environment. Local distortions of the protofibril, however, are also apparent in most samples, and, as discussed in the following subsection, the β-sheet motif is no longer fully recognised by visualisation tools such as VMD implementing automatic approaches[44] to identify the secondary structure of proteins and peptides, as can be seen in Fig. 1 (b).

The nearly constant overall shape and size of the protofibril in all cases and over the entire simulation times suggests to first analyse the protofibril as an elastic body (see Sec. VI in SI), approximating it by an ellipsoid of principal radii a, b, c, and volume $V = 4\pi abc/3$. Analysis

TABLE IV: Radii a, b and c of the ellipsoid of homogeneous density approximating the protofibril shape (see text). Their standard deviation δa, δb and δc are reported as well. All lengths are in Å , the volume of the ellipsoid is in Å ^{3}. Because of the short auto-correlation time, the statistical error on the gyration radii is an order of magnitude smaller than δa, δb, δc. The protofibril orientation with respect to the principal axes of inertia is shown in Fig. S4 of SI. The lowest radius, here called a, corresponds the thickness of the double strand structure. The product of b and c is the area covered by the two sheets. The number of significant digits is consistent with the estimated error bars.

Sample	a	δa	b	δb	c	δc	Vol
SAMP0	11.83	0.15	16.30	0.12	24.62	0.17	19880
SAMP1	11.88	0.18	16.18	0.13	24.73	0.20	19920
SAMP2	12.12	0.23	16.22	0.13	24.66	0.22	20310
SAMP3	11.98	0.20	16.62	0.20	24.68	0.20	20575
SAMP4	11.89	0.10	16.44	0.10	24.67	0.12	20190
SAMP5	12.66	0.23	17.19	0.20	23.53	0.23	21450

of snapshots shows that the orientation of the protofibril with respect to the principal axes of inertia is simple, as shown in Fig. S4 of SI. The changes in the radii and in volume due to the salt addition are small, but the increase of the protofibril volume in SAMP3 and especially in SAMP5 (See Tab. IV) is well above the error bar, and is accompanied, or perhaps caused, by a limited penetration of water (but not of ions) into the protofibril cavity. The high viscosity of SAMP4, due to the high [Tea][Ms] concentration in this sample, limits the variation in the protofibril shape, bringing a, b, c back to their SAMP0 values, and reduces significantly δa, δb, δc.

D. The protofibril secondary structure and H-bonding

The secondary structure of the 5-peptide protofibril has been analysed by reporting the (ϕ, ψ) torsional angles along the peptides' backbone on a Ramachandran plot. For the sake of clarity, we draw separate plots for the β_1 and β_2 sheets, and for the bend, as defined at the beginning of this section. The results for the benchmark SAMP0, given in the left panels of Fig. 5, show that β_1 completely falls into the undistorted β-sheet domains,[45] including the faint spot assigned to LEU17. Already for SAMP0, the plot for β_2 displays additional domains, pointing

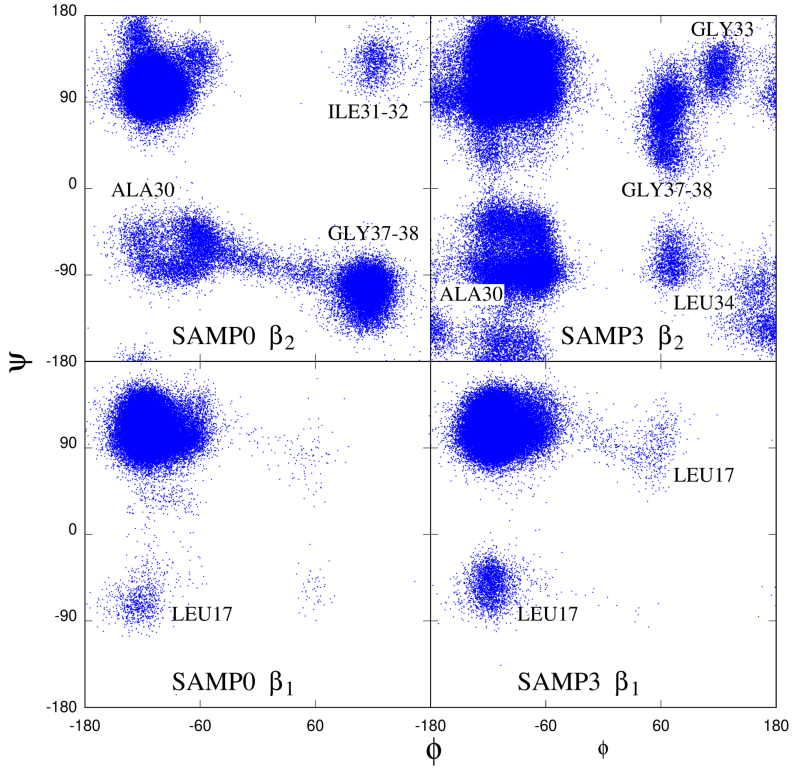

FIG. 5: Ramachandran plot for the β_1 and β_2 sheets of the protofibril in SAMP0 and SAMP3.

to moderate distortions that might also be due to the small size of the simulated protofibril, and the resulting large weight of the under-coordinated A and E peptides. Comparison with the results for SAMP3, given in the right panels of Fig. 5, shows that the β_1 segment is nearly unaffected by the addition of a sizable concentration of [Tea][Ms]. Once again, the plot for β_2 shows much broader structures, whose origin from the geometry of the underlying peptides is easily identified from trajectories. Overall, also for β_2 in SAMP3 the signature of a β-sheet is still recognisable, although, as already stated, distortions are such to violate the criteria used by plotting tools such as VMD to identify the secondary structure (see Fig. 1 (b)). Bends are not as well defined as α-helices or β-sheets, and the Ramachandran plots for the short bend in our samples show a variety of spots limited only by geometric constraints on bonding. The plots for the bend, again for SAMP0 and SAMP3, are given in Fig. S5 in SI. The Ramachandran plot for β_1 and β_2 in SAMP4 of highest [Tea][Ms] concentration (see Fig. S6 in SI) is not significantly different from the SAMP3 plots, showing that the distortion to the secondary structure saturates at some intermediate concentration. The validity of this

observation, however, is made uncertain by the slow dynamics of all species in SAMP4, that might have prevented it from reaching equilibrium, despite the long simulation time.

As a last remark on the Ramachandran plot, we observe that the plot for SAMP5, whose solution contains [Tea][H_2PO_4], is not significantly different from those of SAMP3 at the equivalent [Tea][Ms] concentration (see Fig. S7 in SI). To be precise, the plot for β_1 in SAMP5 is slightly more spread out than in SAMP3, but the plot for β_2 looks similar in the two cases.

To further analyse the protofibril structure, we slightly extend approaches introduced to automatically classify the secondary structure of proteins. Inspired by the Stride[44] algorithm, we assign to each C_α atom in the protofibril a pair of weights $(W_\alpha; W_\beta)$ defined in terms of the corresponding (ϕ, ψ) torsional angles as:

$$W_\alpha = \begin{cases} 1 \text{ if } \quad 180^\circ \leq \phi \leq 10^\circ \text{ and } -120^\circ \leq \psi \leq 45^\circ \\ 0 \quad \text{otherwise} \end{cases} \tag{1}$$

and:

$$W_\beta = \begin{cases} 1 \text{ if } \quad 180^\circ \leq \phi \leq 0^\circ \text{ and } -180^\circ \leq \psi \leq -120^\circ \text{ or } 45^\circ \leq \psi \leq 180^\circ \\ 0 \quad \text{otherwise} \end{cases} \tag{2}$$

In this way, W_α (W_β) is 1 if (ϕ, ψ) fall in the characteristic domain of α-helices (β-sheets) and 0 otherwise. W_α and W_β are mutually exclusive, i.e., only one of them can be 1, and not exhaustive, since they can both vanish for a generic distortion not corresponding, even locally, to either α-helices or β-sheets. We emphasise that these weights alone do not identify β-sheets and α-helices, since that requires also the analysis of H-bonding, but provide a preliminary local characterisation of strands.

The average value of W_α and W_β for the C_α atoms belonging to β_1, β_2 and the bend computed on all the simulated samples are collected in Tab. V. In the control SAMP0 the β-strand signature of β_1 at 0.998% is nearly complete, and the corresponding weight for β_2 is also sizable, although less dominant. The α-helicity weight W_α of β_1 and β_2 is apparently the result of fluctuations, while W_α of the bend is significant. Increasing the [Tea][Ms] concentration up to the 25 wt% of SAMP3 does not affect β_1, but raises significantly the α-helicity of β_2 and, less significantly, of the bend. SAMP5 at 25 wt% concentration of [Tea][H_2PO_4] has an effect similar to that of [Tea][Ms] at the same concentration, showing only a slightly stronger reduction of $W_\beta(\beta_2)$, and (again slightly) larger increase of $W_\alpha(\beta_2)$ and $W_\alpha(bend)$.

To summarize, the α-helicity character of pre-formed protofibrils increases slightly with increasing IL content, [Tea][Ms] and [Tea][H_2PO_4] have similar effect, and in all cases a significant

TABLE V: Average value of the α-helicity and β-sheet index on the C_α atoms of β_1, β_2 and the bend, computed according to Eq. 1 and Eq. 2. The last two rows report the results computed taking into account the pattern of H-bonding, see text.

	SAMP0	SAMP1	SAMP2	SAMP3	SAMP4	SAMP5
$W_\beta(\beta_1)$	0.998	0.94	0.97	0.93	0.94	0.95
$W_\beta(\beta_2)$	0.74	0.74	0.75	0.75	0.75	0.70
$W_\alpha(\beta_1)$	0.00	0.07	0.03	0.04	0.06	0.03
$W_\alpha(\beta_2)$	0.08	0.09	0.08	0.16	0.03	0.20
$W_\alpha(bend)$	0.22	0.20	0.20	0.24	0.18	0.23
	Accounting for H-bonding					
$W_\beta(\beta_1)$	0.81	0.77	0.77	0.78	0.79	0.76
$W_\beta(\beta_2)$	0.66	0.68	0.62	0.41	0.56	0.59

contribution to the α-helicity and its increase upon adding the RTIL salt is given by the bend.

The full identification of α-helices and β-sheets requires the H-bond distribution to match known patterns. For the parallel β_1 sheet, for instance, this corresponds to the H-bonding scheme shown in Fig. 6. Moreover, each segment with the correct angles and H-bonds is counted only if it is at least two residues long. Adding these conditions to the one based on the (ϕ, ψ) angles reduces the β-sheet character of β_1 in SAMP0 from 99.8% to $\sim$ 80%, while for β_2 the reduction is from 75% to 62% (See Tab. V). The reduction in β-sheet character measured in this way is probably somewhat overestimated, since H-bond simulated using empirical force fields are known to break and reform on a short time scale,[46] without separation of the heavier atoms (O, N) involved in the bond. Once again, addition of [Tea][Ms] leaves unchanged the estimate of β-sheet character for β_1, while it reduces the estimate for β_2 down to 50% in SAMP3 and in SAMP4. SAMP5 is slightly less affected.

The same type of analysis based on angles and H-bonds does not find any genuine α-helix structure, because the sequence of amino acids in the bend is too short and too constrained by the junction to β_1 and β_2 to accommodate a helix with correct H-bonding. Nevertheless, the W_α weight defined above remains as an indication of α-propensity.

A major player in the determination of the protofibril secondary structure is the distribution of H-bonds accepted and donated by each peptide to other peptides, to water and to the ions, which is summarised in Tab. VI. Because of the several species and variety of bonding combinations the interpretation of these data is complex, and to enhance readability of the

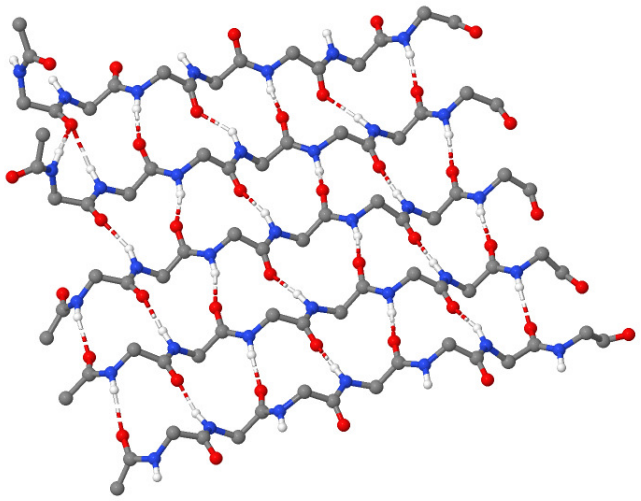

FIG. 6: Pattern of H-bonds characterizing the β_1-sheet of the protofibril. Only backbone atoms and H-bonded hydrogen are shown.

TABLE VI: Average number of peptide-peptide, peptide-water and peptide-ion H-bonds in the simulated samples. The arrow indicates the direction of the proton donation in the H-bond. The total number of engaged donor and acceptor sites on the peptides is given under the label *Total engaged*. Peptide-peptide H-bonds are counted twice in *Total engaged*, since each saturates a donor and an acceptor site.

	SAMP0	SAMP1	SAMP2	SAMP3	SAMP4	SAMP5
Intra-Peptide	0.1	0.1	0.1	0.2	0.0	0.8
Inter-Peptide	73.2	76.9	76.6	61.2	75.9	58.5
Peptide → Water	15.4	13.0	11.9	10.2	5.1	15.3
Water → Peptide	41.3	25.1	33.3	32.8	12.0	37.2
Tot. peptide-Water	56.7	38.2	45.2	43.0	17.1	52.5
Peptide → Anion	0	3.1	5.75	12.5	14.5	6.3
Anion → Peptide	0	0	0	0	0	2.0
Cation → Peptide	0	0.4	0.8	0.9	3.2	2.1
Total engaged	203.3	195.6	205.1	179.1	186.7	179.5

main text it is reported in Sec. VIII of SI.

The main results are that, up to $\sim$ 25 wt% salt concentration, the total number of H-bonds established by the peptides in the protofibril (See *Total engaged* in Tab. VI) decreases slightly upon addition of [Tea][Ms] or [Tea][H_2PO_4], driven by the decrease in the number of

peptide-peptide H-bonds, which is the primary responsible for the change of secondary structure and is the likely reason for the loss of thermodynamic stability of the protofibril quantified in the previous section. The major qualitatively new feature arising from adding [Tea][Ms] or [Tea][H_2PO_4] is the formation of H-bonds donated by peptides to the anions, quantitatively more important for [Tea][Ms] than for [Tea][H_2PO_4]. This effect, and its quantitative difference between $[Ms]^-$ and $[H_2PO_4]^-$, is the most likely cause of the different fibrillation of Aβ peptides in high concentration solutions of the two salts. As a last observation, the number of (accepted+donated) H-bonds joining water to peptides increases slightly upon addition of [Tea][Ms] or [Tea][H_2PO_4]. This last change points to a slight stabilisation of the overall solvation state of the protofibril, or, in other terms, to a weak salting-in effect of either [Tea][Ms] and [Tea][H_2PO_4] on the protofibril.

A secondary but still non negligible role in determining the shape and stability of the protofibril is played by the salt bridge made of an oxygen from ASP23 and the nitrogen from LYS28 joined also by an hydrogen bond. The simulation results (see Tab. S3 in SI) suggest that the intra-peptide bridge is rather stable, and, on average, its stability is enhanced for the center peptides, apparently because the ionic residues are less hydrated (see Tab. S4, S5 in SI). Addition of [Tea][Ms] slowly destabilises the salt bridge, and [Tea][H_2PO_4] has a similar effect. The salt bridge, however, is more stable in SAMP4 than in either SAMP3 or SAMP5, possibly because at the composition of SAMP4 little water is left, decreasing the screening of the positive and negative charges in the bridge. As expected (See Tab. S3, S4 in SI), the bridge on the two external peptides are always the least stable and the most hydrated. It is apparent however that the effect on the salt bridge properties of adding [Tea][Ms] or [Tea][H_2PO_4] is relatively minor.

E. The solvated single peptide and peptide dimer

To enhance our understanding of these systems, the solvation of isolated peptides and peptide dimers has been simulated. Computations for the single peptide in solution, in particular, have been carried out starting from well equilibrated configuration of SAMP0, SAMP3, SAMP4 and SAMP5. In each sample, only one peptide was left in the solution, while the other four were removed and replaced by water, added using the *solvate* tool of Gromacs. For each sample, simulations lasted 300 ns, the last 40 ns of which have been retained for the analysis of

structure, bonding and dynamics. These times cannot be enough to exhaust the intrinsically difficult sampling of a 27 amino acid peptide in water, but they seem to be sufficient to highlight the major H-bonding trends that stabilise the Aβ17-42 peptide in water solutions of [Tea][Ms] and [Tea][H_2PO_4].

A summary of the properties of single peptides in solution is given in Tab. S6 of SI. Besides a few geometric parameters, the most relevant data reported in this table concern the secondary structure and the H-bonding of the peptide.

Analysis of the (ϕ, ψ) angles along the peptide backbone shows that, with respect to SAMP0, the RTIL solution of SAMP3 degrades the β-strand propensity of β_1, leaves β_2 unchanged, and increases significantly the overall α-propensity of the peptide, especially because of the bend contribution. Judging from the (ϕ, ψ) angles, the peptide in SAMP5 is much less changed with respect to SAMP0 than the same peptide in SAMP3. Since the CD measurements on concentrated [Tea][Ms] solutions of Ref. 10,11 are carried out initially on dispersed peptide systems, the results for the secondary structure of single peptides might be as relevant as those discussed in previous sections for the protofibril.

The most promising analysis, however, concerns the H-bonding network, since the structural features, and possibly also the fibrillation properties, seem to reflect the number and distribution of H-bonds donated and accepted by the peptide. Analysis of trajectories for the peptide in SAMP0 shows that about 70% of the proton acceptor and of the proton donor sites on the peptide backbone are saturated at any given time, the most apparent contribution being due to intra-peptide H-bonds. In SAMP3 only $\sim$ 55% of the H-bonding capability is saturated. The decrease with respect to SAMP0 is due primarily to the low number of intra-peptide bonds, while the number of bonds matching the peptide to the environment increases by a few units. More importantly, in SAMP3 the proton donation by the peptide to $[Ms]^-$ plays a major role, paralleling the bonding picture observed for the protofibril. The close association of the peptide with $[Ms]^-$, driven by multiple H-bonds, is a remarkable aspect in all the simulated [Tea][Ms] / water samples, and is apparent already from snapshots (see Fig. 7). It is worth pointing out that the average number of peptide-$[Ms]^-$ H-bonds is only $\sim$ 30% lower than the number for the five-peptide protofibril, emphasising the fact that the $[Ms]^-$ bonding occurs preferentially at the extremal peptides, while intermediate peptide are much less concerned. SAMP5 shows similar but weaker changes with respect to SAMP0 than SAMP3, since the decrease of intra-peptide and peptide-water H-bonding is less than in SAMP3, while, at the

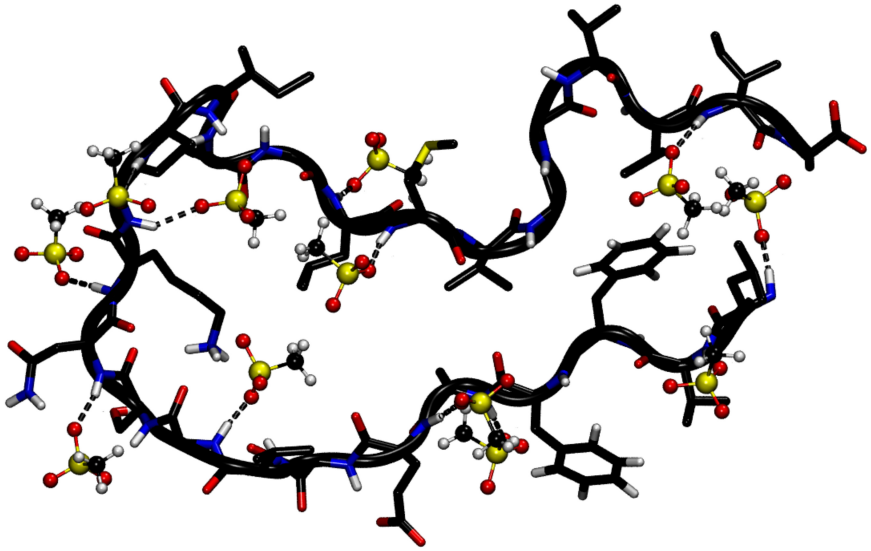

FIG. 7: Snapshot of a single peptide in SAMP4, decorated by hydrogen bonded $[Ms]^-$ anions.

same time, the peptide bonding to anions is less important. It is tempting to speculate that the close coordination of the peptide by $[Ms]^-$ through H-bonding plays a role in stabilising the solvated state of single peptides in [Tea][Ms] / water solutions, preventing fibrillation at high [Tea][Ms] concentration. The condensation of anions on the already negatively charged peptide is remarkable, but complex arrangements of like-charge ions have already been identified in protic ionic liquids.[47] In our systems, the aggregation of like-charge ions is favored by the presece of water and of the protofibril, increasing the role of the hidrogen bonding network. Moreover, the ion density in SAMP3 and SAMP5 is apparently sufficient to provide a robust screening of electrostatic interactions, as shown by the analysis of the electrostatic potential around the peptides, whose spherical average is shown in Fig. 8.

Simulations have also been carried out for the single peptide in SAMP4 with the highest concentration of [Tea][Ms]. The results of 300 ns simulations show that the structural results for the peptide in SAMP4 are in between those of SAMP0 and SAMP3, very likely because of the exceedingly slow kinetics of this system, precluding its equilibration.

The leads gained by the single peptide simulations are confirmed and therefore reinforced by the results of simulations of peptide dimers in the same SAMP0, SAMP3, SAMP4 and SAMP5 solutions, summarised in Tab. S7 of SI. These simulations have been carried out starting again from the protofibril in the corresponding equilibrated samples, following the same protocol

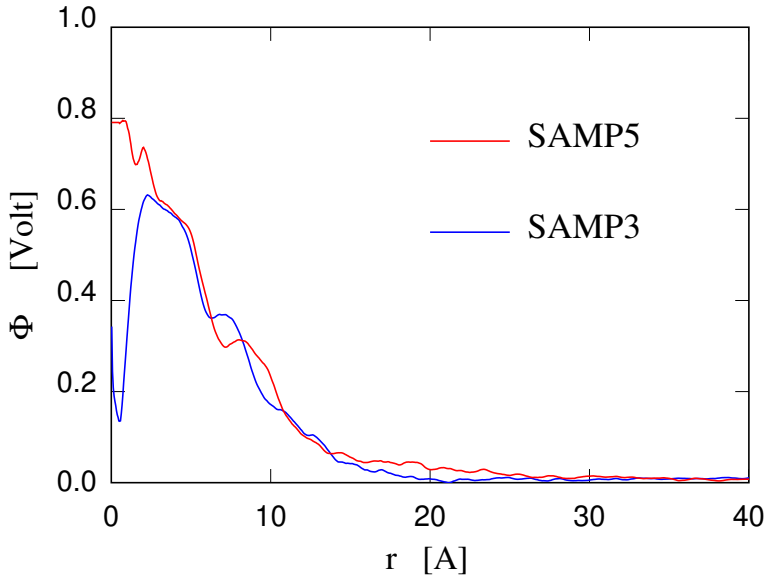

FIG. 8: Spherical average of the electrostatic potential around a single peptide in the SAMP3 and SAMP5 solutions. The origin corresponds to the peptide centre of mass. All charges (peptide, water, ions) are taken into account. In both cases, the electrostatic potential gives origin to a force attracting negative charges towards the peptide.

and simulation times used for the single peptide. We emphasise that in all cases the dimer starts from a bound parallel configuration, with pre-formed H-bonds and salt bridges. The results are quantitatively different but still consistent with those of the single peptide. The β_1 segment is weakly affected by adding the RTIL salts, the β_2 segment is somewhat more distorted, α-helicity increases in SAMP3 and SAMP5 with respect to the SAMP0 case, and the α-character is acquired mainly by the *bend*. Animations of trajectories show that the most apparent loss of structural and H-bonding features with respect to the protofibril case occurs in SAMP0, with a partial separation and refolding of the two peptides. In the other cases, a remnant of the original protofibril structure is left. Once again, these observations are likely to reflect the distribution of H-bonds surrounding the peptides. As expected, the role of the inter-peptides H-bonding is significantly less than in the protofibril case, and intra-peptide bonding is virtually absent. Moreover, the H-bonding between the peptides and the anions is again a relevant feature, especially for the [Tea][Ms] solutions. More importantly, the total

number, i.e., considering both peptides, of anions H-bonded to the peptides in the dimer is neither much higher than in the single peptide case nor much lower than in the protofibril case. This observation confirms that the number of anions bound to a fibril increases only slowly with the number of peptides, since anion H-bonding occurs preferentially at the two extremal peptides. This feature, once again quantitatively more important for the [Tea][Ms] samples, might underlie the relative stabilisation of single peptides with respect to fibrils. It might also greatly affect the kinetics of peptide addition to or removal from a fibril.

The role of peptide-anion H-bonding in stabilizing single peptides in RTIL solution prompted us to investigate how this feature evolves during the separation of one peptide from the protofibril, simulated in the previous section. Analysis of trajectories collected during US shows that the peptide refolding and decoration by additional anions takes place only slowly with increasing separation. This observation points to interactions and correlations active on distances of a few nm due to the complex structure of peptides, water and RTIL ions, possibly enhanced by the nanostructuring of the solution.

F. Thioflavin-T binding

Thioflavin-T (ThT^+) is the dye of choice to detect a wide variety of amyloid aggregates, whose sensing ability is due to a $\sim$ 1000-fold increase in the luminescence of this molecule upon adsorption on the surface of an amyloid fibre. Different mechanisms have been proposed to explain this selective luminescence. A widely accepted explanation is that the luminescence of ThT^+ in solution is quenched by a fast non-radiative transition, due to a rotational mode. The proximity of the fibril restrains this motion, and amplifies the radiative decay of the optically excited state of the dye. To strengthen the connection of our simulations with experiments, we investigated the dependence of ThT^+ binding to the protofibril on the presence of [Tea][Ms]. To this aim, we replaced by ThT^+ one cation in the benchmark sample SAMP0 and in SAMP3.

In both cases, simulations started with the single ThT^+ ion as far from the protofibril ($\sim$ 50 Å from the protofibril centre of mass, $\sim$ 30 Å from its surface) as compatible with our periodic boundary conditions, and each sample has been simulated for at least 400 ns.

In SAMP0, following a short equilibration of a few ns, ThT^+ found its way to the protofibril surface. In agreement with experimental findings,[48] it accommodates itself perpendicular to the growth direction of the protofibril (See Fig. 9 (a)), along the groove formed by VAL18-PHE19-

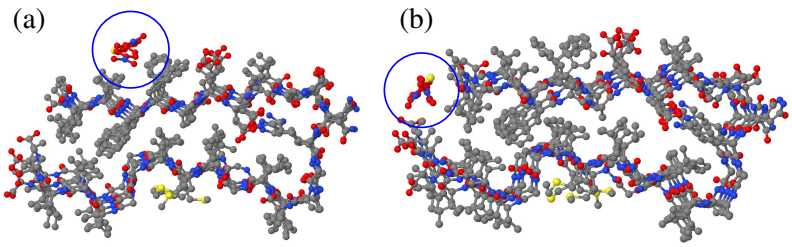

FIG. 9: Adsorption pose of ThT^+ on the protofibril in the control [Na][Cl] solution of SAMP0. (a) Pose reached within a few ns after inserting ThT $\sim$ 60 nm away from the protofibril centre of mass. (b) Pose assumed after 200 ns equilibration. Carbon atoms on ThT^+ have been painted red, and hydrogens are not shown.

PHE20. After further 200 ns, it moved to the open mouth of the c-shaped protofibril (See Fig. 9 (b)), where it remained until the end of the simulation. In this second location, ThT^+ is parallel to the protofibril growth axis. The first location is apparently favored by the relatively short distance from the anionic charge of the neighboring GLU22 and by the gain of dispersion energy due to the proximity of the PHE-aromatic rings. The second location is apparently stabilised by the Coulomb interaction with the negatively charged ALA42 termination. No evidence for this location is given by experimental papers, hence it might be an artifact of our model due to the choice of a fully deprotonated C-terminus, or to the small size of the protofibril. It might also be that in this second location ThT^+ does not contribute to luminescence, therefore it is not detected by experiments. Because of the slow rate of interchange between the two binding poses (only one event was observed) we are unable to assess the relative stability of the two sites without an explicit and costly free energy computation.

The evolution of ThT^+ in SAMP3 has been different. First, it took $\sim$ 150 ns to reach the protofibril. This could be explained in terms of Coulomb interactions, since, at variance from SAMP0, in SAMP3 ThT^+ is just one of more than 250 cations, the negative charge of the protofibril is heavily screened, and there is no long range force driving ThT^+ to the protofibril. Once ThT^+ reaches the protofibril surface, the association is not permanent, but several association and dissociation events are observed. When adsorbed, ThT^+ does not occupy the groove or the open protofibril termination, but it moves over the surface, with, however, a preference for the side of the protofibril (See Fig. 10). Also this loss of binding

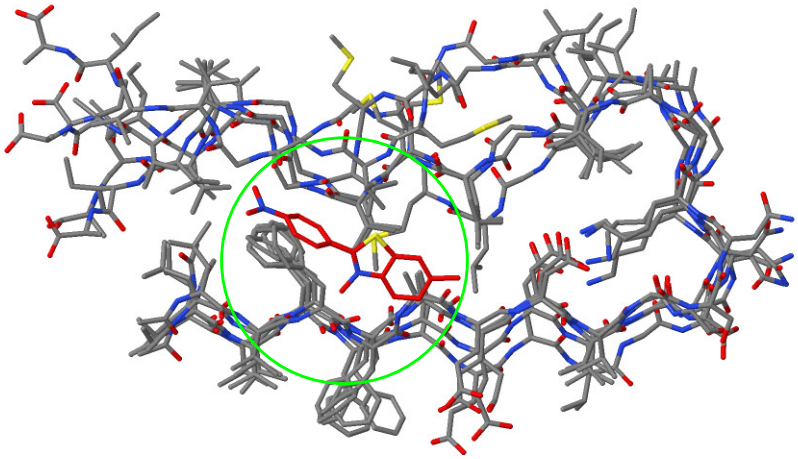

FIG. 10: Adsorption pose of ThT on the side of the protofibril in SAMP3. Carbon atoms on ThT^+ have been painted red, and hydrogens are not shown.

cohesion may be due to the competition of ThT^+ with the many cations located in proximity of the protofibril. In a population of long fibres, the density of absorption sites on the fibril side is negligible, making the binding of ThT^+ to the fibril even more tenuous.

According to Ref. 49, the quenching of luminescence in solution is related to rotations around the central C-C single bond of ThT^+, while the other single bond, i. e., C-N, seems to have only an auxiliary role. In our simulations, we observe many rotational isomerisations around the central C-C single bond, without an apparent effect due to the absorption of ThT^+ on the protofibril, or to the different adsorption locations.

To summarise, our simulations point out that in the presence of complex salts at non-negligible concentration, the ThT^+ ion has to compete with many other cations to bind to the fibril, whose negative charge, moreover, is increasingly screened with increasing salt concentration. In estimating the degree of aggregation from luminescence, therefore, the dependence on salt concentration of the ThT^+ affinity for and binding pose on the fibril should be taken into account.

IV. SUMMARY AND DISCUSSION

The present study has been motivated by experimental measurements investigating the effect of protic ionic liquids on the fibrillation of Aβ peptides,[10,11] showing that at high (> 70 wt%)

TABLE VII: Overview of the analyses and results reported in the paper

Analysis	**[Tea][Ms]**	**[Tea][H_2PO_4]**	**Observation**
H-bonding ions-water	Strong H-bond donation water $\rightarrow [Ms]^-$ $[Tea]^+ \rightarrow$ water	Strong H-bond donation $[Tea]^+ \rightarrow [H_2PO_4]^-$	Weaker dissociation in water and reduced ionic character of [Tea][H_2PO_4] with respect to [Tea][Ms]
Protofibril geometry	Increase of the protofibril's volume of 3.5%	Increase of the protofibril's volume of 7.9%	Percentage computed for SAMP3 and SAMP5 with respect to SAMP0
Protofibril secondary structure	Partial loss of β-character Modest increase of α-character		Part of the α-character increase is due to the bend
H-bonding ions-protofibril	Strong H-bond donation peptides $\rightarrow [Ms]^-$	Weaker H-bond donation peptides $\rightarrow [H_2PO_4]^-$	This is the likely cause of the different Aβ fibrillation in high salt concentration
Free energy	Binding free energy of peptides decreased by 21 kcal/mol in SAMP3	Binding free energy of peptides decreased by 14 kcal/mol in SAMP5	See Tab. III Qualitative agreement with experimental results of Ref. 10
Single peptide secondary structure	Decrease of the β-character of β_1 Unchanged β-character of β_2 Increase of the α-character of the protofibril		The degradation of the secondary structure due to [Tea][H_2PO_4] is less pronounced
Single peptide H-bonding	Strong H-bond donation peptides $\rightarrow [Ms]^-$	Weaker H-bond donation peptides $\rightarrow [H_2PO_4]^-$	Results in line with those obtained for the protofibril
Peptide dimer Secondary structure	Increase of the α-character of the dimer		Most of the effect is due to the bend
Peptide dimer H-bonding	Strong H-bond donation peptides $\rightarrow [Ms]^-$	Weaker H-bond donation peptides $\rightarrow [H_2PO_4]^-$	Results in line with those obtained for the protofibril

concentration [Tea][Ms] prevents fibrillation, and [Tea][H_2PO_4] favours it. Our study does not (and could not) aim at a direct comparison with experiment, but, rather, it explores a variety of properties and features related to the experimental systems and phenomena looking for thermodynamic and bonding trends that support the destabilisation of Aβ fibrils by [Tea][Ms] and that could explain the different effect of [Tea][H_2PO_4]. To this aim, atomistic simulations based on the Gromos force field have been carried out for samples consisting of a protofibril made of five Aβ17-42 peptides prepared and equilibrated in a parallel β-sheet configuration, embedded into a water solution of [Tea][Ms] or [Tea][H_2PO_4]. A control sample with a dilute [Na][Cl] solution has been simulated as well. The scan of salt concentrations has been limited by large fluctuations in the distribution of ions at intermediate concentrations due to marked nanostructuring of the RTIL / water solutions,[40] and by slow dynamics at high concentrations,

in practice preventing full equilibration of the system. To help connecting the several different aspects analysed in our study, a schematic summary is provided in tabular form (See Tab. VII).

First of all, the thermodynamic stability of the protofibril, and its kinetics of formation and dissolution have been assessed by the determination of the free energy profile along a reaction coordinate measuring the separation of a single peptide from the remaining 4-peptide protofibril. Moreover, plain MD simulations in the NPT ensemble have been used to probe the stability of the protofibril, characterised by a variety of structural properties, such as the overall shape of the protofibril, the Ramachandran plot of the (ϕ, ψ) angles for all C_α atoms in the peptides, the classification of the secondary structure of the protofibril, the distribution and quality of the H-bonds among peptides, water and ions.

The results show several intriguing points of contact between simulations and experiments.

For instance, the computation of the free energy ΔF energy required to detach one peptide shows that already at 25 wt% concentration, the RTIL addition decreases the protofibril stability with respect to the control sample, and the effect is significantly more pronounced for [Tea][Ms] than for [Tea][H_2PO_4]. This shift of chemical equilibrium in favour of solvated peptides in the [Tea][Ms] / water samples is consistent with the experimental observation of slow dissolution of Aβ40 fibrils in pure [Tea][Ms],[13] taking place while the morphology of the remaining fibrils remains unchanged. Moreover, again in qualitative agreement with the experimental evidence, over a broad concentration range the addition of [Tea][Ms] or [Tea][H_2PO_4] affects the secondary structure of the 5-peptide amyloid protofibril, enhancing its α-helicity, especially in the bend segment joining the two β strands that characterize the fibril.

Simulations of single peptides and peptide dimers in the same solutions of the protofibril confirm the increase of the α-propensity with increasing salt concentration, especially for [Tea][Ms], that might affect the nucleation and growth of fibrils from a population of peptides in solution.

However, the reach of our study is somewhat limited by the fact that time- and size-scale limitations still prevent our computational approaches from covering the highest salt concentrations considered in the experiment, and thus simulation cannot reproduce directly the qualitatively different effect of [Tea][Ms] and [Tea][H_2PO_4], nor it can provide evidence for a drastic change of fibrillation properties at salt concentrations exceeding ~ 70 wt%, as seen in experiments.

Nevertheless, the computational results provide a number of clues on the interpretation of the experimental results, beyond the strict limits of size, time and salt concentration that affect

simulation. First of all, judging from H-bonding, [Tea][Ms] is significantly more dissociated in water, hence more ionic, than [Tea][H_2PO_4]. If the ability of RTILs to affect fibrillation is related to their ionic strength, then the difference between [Tea][Ms] and [Tea][H_2PO_4] is no longer a surprise. A second relevant observation is that the change in binding free energy of peptides, estimated here for [Tea][Ms] and [Tea][H_2PO_4] solutions at ~ 25 wt% concentration, could easily explain the different fibrillation properties if extrapolated to concentrations $>$ 80%. A third major feature revealed by simulation is the close association of peptides with $[Ms]^-$ and $[H_2PO_4]^-$ anions through H-bonding, quantitatively more important for $[Ms]^-$ than for $[H_2PO_4]^-$. The significance of these observations with respect to fibrillation is confirmed by the simulations for isolated peptides and for peptide dimers in the same solutions of the protofibrils, suggesting that the destabilisation of the protofibril by RTILs might be attributed to the competing stabilisation of isolated peptides in solution, due to their extensive H-bonding with anions. Once again, this preferential binding is stronger for $[Ms]^-$ than for $[H_2PO_4]^-$, reinforcing the identification of the anion-peptide binding as the mechanism underlying the relative destabilisation of the protofibril.

To complement these primary issues, NPT-MD simulations have been carried out to investigate the effect of [Tea][Ms] on the binding of the ThT^+ fluorescent molecule used in experiments to probe fibrillation in Aβ peptide solutions. Simulation results show that the binding of the cationic marker is significantly perturbed and weakened by the competition with the RTIL ions, both cations and anions. Hence, the effect of adding salt on the efficiency of the fluorescent marking has to be taken into account in assessing the fibrillation kinetics of Aβ peptides in salt solutions.

A further feature to be taken into account is the homogeneity of the solution at the molecular scale. In our simulations, the solution is homogeneous on average, and a phase separation can be excluded for the salt / water concentrations that have been simulated. However, large fluctuations in the ion distribution point to nanostructuring of the water/organic salt solution, whose presence could greatly affect the fibrillation process. First, the local concentration of ions, and especially anions in proximity of peptides and their fibrils could differ significantly from the nominal average composition. Moreover dynamical processes such as diffusion could be affected in a different way on different length scales, opening the way to a broad variety of effects on fibrillation by organic ionic liquids that could be exploited for biomedical and nanotechnology applications.

As a last remark, we comment once again on limitations of the model that could have affected our simulations in their comparison with experiments. The rigid (i.e., unpolarisable) ion force field model is still crucial for simulating the large samples and long times required by the present study. However, polarisability of all species, and anions in particular, is certainly very important for the systems we investigated. Moreover, the associated/dissociated state of all titratable acidic groups in the system might change upon adding RTILs at high concentration, especially for protic ionic liquids. Because of the availability of detailed and accurate experimental measurements, the problem we analysed could represent a useful playground to quantify the effect of these model limitations, and to validate higher-order models.

ACKNOWLEDGMENTS - A.B. acknowledges support from Science Foundation Ireland (grant no. 15-SIRG- 3538), and from the Italian Ministry of Education, University and Research (grant no. MIUR-DM080518-372).

Conflicts of interest: There are no conflicts of interest to declare.

---

[1] Hallett, J. P.; Welton, T. Room-temperature ionic liquids: Solvents for synthesis and catalysis. 2. *Chem. Rev.* **2010**, *111*, 3508-3576.

[2] Ventura, S. P. M.; e Silva, F. A.; Quental,M. V.; Mondal, D.; Freire, M. G.; Coutinho, J. A. P. Ionic-liquid-mediated extraction and separation processes for bioactive compounds: Past, present, and future trends. *Chem. Rev.* **2017**, *117*, 6984-7052.

[3] Hough, W. L.; Smiglak, M.; Rodríguez, H.; Swatloski, R. P.; Spear, S. K.; Daly, D. Y.; Pernak, J.; Grisel, J. E.; Carliss, R. D.; Soutullo, M. D.; Davis, J. H., Jr.; Rogers, R. D. The third evolution of ionic liquids: active pharmaceutical ingredients. *New J. Chem.* **2007**, *31*, 1429-1436.

[4] Pedro, S. N.; Freire, C. S. R.; Silvestre, A. J. D.; Freire, M. G. The role of ionic liquids in the pharmaceutical field: An overview of relevant applications. **Int. J. Mol. Sci. 2020**, *21*, 8298.

[5] Egorova, K. S.; Gordeev, E. G.; Ananikov, V. P. Biological activity of ionic liquids and their application in pharmaceutics and medicine. *Chem. Rev.* **2017**, *117*, 7132-7189.

[6] Benedetto, A.; Ballone, P. Room-temperature ionic liquids and biomembranes: setting the stage for applications in pharmacology, biomedicine, and bionanotechnology. *Langmuir* **2018**, *34*, 9579-9597.

[7] Byrne, N.; Angell, C. A. Formation and dissolution of hen egg white lysozyme amyloid fibrils in protic ionic liquids. *Chem. Commun.* **2009**, 1046-1048.

[8] Takeiyo, T.; Yoshimura, Y. Suppression and dissolution of amyloid aggregates using ionic liquids. *Biophys. Rev.* **2018**, 852-860.

[9] Pillai, V. V.; Benedetto, A. Ionic liquids in protein amyloidogenesis: a brief screenshot of the state-of-the-art. *Biophys. Rev.* **2018**, 847-852.

[10] Debeljuh, N.; Barrow, C. J.; Henderson, L.; Byrne, N. Structure inducing ionic liquids - Enhancement of alpha helicity in the Abeta(1-40) peptide from Alzheimer's disease. *Chem. Commun.* **2011**, *47*, 6371-6373.

[11] Debeljuh, N.; Barrow, C. J.; Byrne, N. The impact of ionic liquids on amyloid fibrillation of Aβ16-22: tuning the rate of fibrillation using a reverse Hofmeister strategy. *Phys. Chem. Chem. Phys.* **2011**, *13*, 16534-16536.

[12] Murphy, M. P.; LeVine, H. Alzheimers disease and the β-amyloid peptide. *J. Alzheimers Dis.* **2010**, *19*, 311-323.

[13] Debeljuh, N.-J. Amyloid peptide self assembly in protic ionic liquids. Ph.D. thesis, Deakin University, 2014.

[14] Chen, G.; Xu, T.; Yan, Y.; Zhou, Y.; Jiang, Y.; Melker, K.; Xu, H. E. Amyloid beta: structure, biology and structure-based therapeutic development. *Acta Pharmacol. Sin.* **2017**, *38*, 1205-1235.

[15] Greaves, T. L.; Drummond, C. J. Protic ionic liquids: Properties and applications. *Chem. Rev.* **2008**, *108*, 206-237.

[16] Greaves, T. L.; Drummond, C. J. Protic ionic liquids: Evolving structure-property relationship and expanding applications. *Chem. Rev.* **2008**, *108*, 206-237.

[17] Byrne, N.; Wang, L.-M.; Belieres, .-P.; Angell, C. A. Reversible folding-unfolding, aggregation protection, and multi-year stabilization, in high concentration protein solutions, using ionic liquids. *Chem. Commun.* **2007**, 2714-2716.

[18] Greenfield, N. J. Using circular dichroism spectra to estimate protein secondary structure. *Nat. Protoc.* **2006**, *1*, 2876-2890.

[19] Vassar, P. S.; Culling, C. F. Fluorescent stains with special reference to amyloid and connective tissues. *Arch. Pathol.* **1959**, *68*, 487-498.

[20] LeVine, H. Thioflavine T interaction with synthetic Alzheimer's disease beta-amyloid peptides: detection of amyloid aggregation in solution. *Protein Sci.* **1993**, *2*, 404-410.

[21] Ban, T.; Hamada, D.; Hasegawa, K.; Naii, H.; Goto, Y. Direct observation of amyloid fibril growth monitored by thioflavine T fluorescence. *J. Biol. Chem.* **2003**, *278*, 16462-16465.

[22] Zhang, Y.; Cremer, P. S. Interactions between macromolecules and ions: the Hofmeister series. *Current Opinion in Chem. Biol.* **2006**, *10*, 658-663.

[23] Nasica-Labouze, Nguyen, P. H.; Sterpone, F.; Berthoumieu, O.; Buchete, N.-V.; Cot'e, S.; De Simone, A.; Doig, A. J.; Faller, P.; Garcia, A.; *et al.* Amyloid β protein and Alzheimers disease: When computer simulations complement experimental studies. *Chem. Rev.* **2015**, *115*, 3518-3563.

[24] Illig, A.-M.; Strodel, B. Performance of Markov state models and transition networks on characterizing amyloid aggregation pathways from MD data. *J. Chem. Theor. Comput.* **2020**, *16*, 7825-7839.

[25] Lemkul, J. A.; Bevan, D. R. Assessing the stability of Alzheimer amyloids protofibrils using molecular dynamics. *J. Phys. Chem.B* **2010**, *114*, 1652-1660.

[26] Lührs, T.; Ritter, C.; Adrian, M.; Riek-Loher, D.; Bohrmann, B.; Döbeli, H.; Schubert, D.; Riek, R. 3D structure of Alzheimer's amyloid-β(142) fibrils. *Proc. Natl. Acad. Sci. USA* **2005**, *102*, 17342-17347.

[27] Malde, A. K.; Zuo, L.;, Breeze, M.; Stroet, M.; Poger, D.; Nair, P. C.; Oostenbrink, C.; Mark, A. E. An automated force field topology builder (ATB) and repository: version 1.0. *J. Chem. Theory Comput.* **2011**, *7*, 4026-4037.

[28] Essmann, U.; Perera, L.; Berkowitz, M. L. Darden, T.; Lee, H.; Pedersen, L. A Smooth Particle Mesh Ewald Method. *J. Chem.Phys.* **1995**, *103*, 8577-8593.

[29] Jmol: an open-source Java viewer for chemical structures in 3D. http://www.jmol.org/ accessed: 30 November 2020.

[30] Humphrey, W.; Dalke, A.; Schulten, K. VMD - Visual Molecular Dynamics *J. Molec. Graphics* **1996** *14*, 33-38.

[31] Kumar, S.; Rosenberg, J. M.; Bouzida, D.; Swendsen, R. H.; Kollman, P. A. The weighted histogram analysis method for free-energy calculations on biomolecules. I. The method. *J. Comput. Chem. 1992*, *13*, 1011-1021.

[32] Hub, J. S.; de Groot, B. L.; van der Spoel, D. g_wham - A free weighted histogram analysis implementation including robust error and autocorrelation estimates. *J. Chem. Theory Comput.* **2010**, *6*, 3713-3720.

[33] Pandian, T. S.; Cho, S. J.; Kang, J. Dihydrogen phosphate as a hydrogen-bonding donor element: anion receptors based on acylhydrazone. *J. Org. Chem.* **2013**, *78*, 12121-12127.

[34] W. Kunz, W.; Lo Nostro, P.; Ninham, B. W. The present state of affairs with Hofmeister effects. *Curr. Opin. Colloid Interface Sci.* **2004**, *9*, 1-18.

[35] Weingärtner, H.; Cabrele, C.; Herrmann, C. How ionic liquids can help to stabilize native proteins. *Phys. Chem. Chem. Phys.* **2012**, *14*, 415-426.

[36] Tietze, A. A.; Bordusa, F.; Giernoth, R.; Imhof, D.; Lenzer, T.; Maaß, A.; Mrestani-Klaus, C.; Neundorf, I.; Oum, K.; Reith, D.; Stark, A. On the Nature of Interactions between Ionic Liquids and Small Amino-Acid-Based Biomolecules. *ChemPhysChem* **2013**, *14*, 4044-4064.

[37] Jiang, H. J.; Atkin, R.; Warr, G. G. Nanostructured ionic liquids and their solutions: Recent advances and emerging challenges. *Curr. Opin. Green and Sustainable Chem.* **2018**, *12*, 27-32.

[38] Greaves, T. L.; Kennedy, D. F.; Weerawardena, A., Tse, N. M. K.; Kirby, N.; Drummond, C.J. Nanostructured protic ionic liquids retain nanoscale features in aqueous solutions while precursor Brønsted acids and bases exhibit different behaviour. *J.Phys. Chem. B* **2011**, *115*, 2055-2066.

[39] Han, Q.; Wang, X.; Byrne, N. Utilizing water activity as a simple measure to understand hydrophobicity in ionic liquids. *Frontiers in Chem.* **2019**, *7*, 12.

[40] Pallavi, K.; Pillai, V.; Gobbo, V.; Ballone, P.; Benedetto, A. The transition from salt-in-water to water-in-salt nanostructures in water solutions of organic ionic liquids relevant for biological applications. *Phys. Chem. Chem. Phys. in press.* doi: 10.1039/D0CP04959J

[41] MacFarlane, D. R.; Chong, A. L.; Forsyth, M.; Kar, M.; Vijayaraghavan, R.; Somers, A.; Pringle, J. M. New dimensions in salt-solvent mixtures: a 4th evolution of ionic liquids. *Faraday Discuss.* **2018**, *206*, 9-28.

[42] Azov, V. A.; Egorova, K. S.; Seitkalieva, M. M.; Kashin, A. S.; Ananikov, V. P. "Solvent-in-salt" systems for design of new materials in chemistry, biology and energy research. *Chem. Soc. Rev.* **2018**, *47*, 1250-1284.

[43] Sashi, P.; Bhuyan, A. K. Viscosity dependence of some protein and enzyme reaction rates: seventy-five years after Kramers. *Biochem.* **2015**, 4453-4461.

[44] Frishman, D.; Argos P. Knowledge-based protein secondary structure assignment. *Proteins: Struct., Funct., Genet.* **1995**, *23*, 566-579.

[45] J. M. Berg, J. L. Tymoczko, and L. Stryer, *Biochemistry*, 7th Edition, W.H. Freeman, New York (2012).

[46] Luzar, A.; Chandler, D. Effect of environment on hydrogen bond dynamics in liquid water. *Phys. Rev. Lett.* **1996**, *76*, 928-931.

[47] Niemann, T.; Zaitsau, D. H.; Strate, A.; Stange, P.; Ludwig, R. Controlling "like-likes-like" charge attraction in hydroxy-functionalized ionic liquids by polarizability of the cations, interaction strength of the anions and varying alkyl chain length. *Phys. Chem. Chem. Phys.* **2020**, *22*, 2763-2774.

[48] Krebs, M. R. H.; Bromley, E. H. C.; Donald, A. M. The binding of thioflavin-T to amyloid fibrils: localisation and implications. *J. Struct. Bio.* **2005**, 30-37.

[49] Srivastava, A.; Singh, P. K.; Kumbhakar, M.; Mukherjee, T.; Chattopadyay, S.; Pal, H.; Nath, S. Identifying the bond responsible for the fluorescence modulation in an amyloid fibril sensor. *Chem. Eur. J.* **2010**, *16*, 9257-9263.